PAPER

Multiple interferometer interaction free measurement using polarized light

IOP Publishing Journal of Physics B: Atomic, Molecular and Optical Physics
J. Phys. B: At. Mol. Opt. Phys. **49** (2016) 045501 (8pp) doi:10.1088/0953-4075/49/4/045501

Multiple interferometer interaction free measurement using polarized light

Jin Wang, Kevin Pitt and Michael Milgie

University of Michigan-Dearborn, 4901 Evergreen Rd., Dearborn, MI 48128, USA

E-mail: jinwang@umich.edu

Received 12 July 2015, revised 26 October 2015
Accepted for publication 26 October 2015
Published 25 January 2016

Abstract

This paper experimentally and theoretically investigates improving interaction free measurement (IFM) efficiency using a chain of multiple interferometers with transmissive beam splitters of reflectivity less than 50%. The object measured with IFM is present or absent from one of the interferometer paths depending on the polarization of the incident light. The ability to effectively move an object in and out of the system without physically moving it makes implementing a multiple chain interferometer more practical. It also allows verifying the desired interferometer phase while simultaneously making the IFM measurement. A recursive phase model of a chain of interferometers is presented which accounts for both losses and arbitrary phase differences between each pair of arms in the chain. The recursive model predicts the photodiode power and is experimentally validated for a chain of interferometers of lengths one and two.

Keywords: optical interferometry, optical polarization, interaction free measurement

(Some figures may appear in colour only in the online journal)

1. Introduction

One limitation that quantum mechanics has imposed is that the disturbance to a system by measuring it cannot be smaller than a certain amount or quanta. This limitation is not present in a classical view since a disturbance can be arbitrarily small. Renninger was the first to theorize that a system could potentially be measured indirectly without disturbing it at all [1]. Later, Dicke [2] described how the non-interaction between photons and an atom modifies the probability wave function of the atom. Then Elitzur and Vaidman (EV) [3] proposed an 'interaction free measurement' (IFM) experiment that could be carried out using a Mach–Zehnder interferometer to measure the presence or absence of a completely opaque object without a single photon absorbed by the object. The two beam splitters in the EV interferometer have reflection to transmission ratios that can be varied from 50:50 to 100:0. As the beam splitter reflectivities deviate from 50%, the probability of detecting a bomb that will explode if it absorbs a single photon without setting it off increases from 25% to a limit of 50%.

One solution to the 50% IFM probability limit of the single interferometer is a system or chain of coupled Mach–Zehnder interferometers [4]. The coupled interferometers increase the probability of photons to perform measurement of the presence of an object without being absorbed by the object as the number of interferometers increases. If the object is present, the light behaves as a particle and will follow the path without the object to the 'light port'. If there is no object present and the beam splitters have the correct reflectivity, the photons behave as a wave and can be tuned to constructively interfere into the path that would without interference be the path of minimum light intensity. The minimum light intensity path ends at the 'dark port'.

This paper investigates the experimental implementation of a multiple interferometer IFM chain using transmissive beam splitters with reflectivity less than 50%. The idea to implement an IFM chain to obtain high efficiency IFM measurements using beam splitters with reflectivity greater than 50% has been previously suggested [4]. The setup is displayed in figure 2. The object used to perform IFM measurements upon is a photodiode 'bomb' at the vertically polarized output of a polarization beam splitter. This object will be in the path when the light is vertically polarized, and is removed from the path if the light is horizontally polarized. When the incident light is diagonally polarized the object can be measured in and out of the path at the same time depending on the photon polarization. This allows verifying in real time

whether the interferometer arm lengths are correctly aligned while making an IFM measurement. The real time diagnostic is advantageous if IFM is to be used on turbid media such as biological tissue that changes the phase relationship on a millisecond time frame [5]. The ability to diagnose the IFM chain phases becomes more important as the number of interferometers in the chain is increased.

One experiment that could benefit from a polarization sensitive object is an integrated quantum photonic chain of ten interferometers [6]. Since the photonic circuit is not changeable after it is manufactured, an absorbing object is placed into the interferometer arms by either placing the objects with single nanometer position near each arm, or manufacturing nearly identical chips one with absorbers and the other without absorbers. These two options do not allow switching the object quickly in and out of the system. However, by using a polarization dependent object, the object can be switched in and out of the system with high speed since there is no need to move physical objects in and out of the system. A second IFM experiment using electrons instead of photons to implement an IFM scheme [7] may also be adapted to a similar scheme by controlling the orientation of the electron spin and using an electron spin dependent object instead of a polarization dependent object. Another IFM experiment uses Rubidium atoms pumped into a state causing them to be polarization dependent which is similar to the polarization dependent object used in this paper [8]. This results in photons that are 95% resonant with Rubidium atoms that can be used in Rubidium atom based quantum memories. A similar IFM approach could be applied to generating photons for use in quantum dot based memory [9].

This paper also introduces a recurrence equation using phase vectors to predict the photodiode power of IFM experiments using multiple interferometers in a chain. The recurrence model accounts for an arbitrary number of interferometers, arbitrary beam splitter reflectivities, beam splitter losses, object losses and phase differences between each pair of interferometer arms The recursive model is an alternative method [10] that can be used to find the phase change caused by a system of objects. The recursive model and the experimental results of the interferometer chain lengths one and two are compared and found to agree.

2. The single interferometer setup

The two experimental setups investigated in this paper consist of interferometer chains of length one and two. This section describes the experimental setup of the single interferometer and the polarization light source.

The polarization controlled light source used in IFM setups is shown in figure 1. The laser is a 5 mW 632.8 nm HeNe TEM_{00} with random polarization. Although the coherence length of the laser can affect the visibility of the interference by a few percent, the IFM results are not affected since the IFM efficiency is measured when the object is present and no interference occurs. The horizontal polarization is selected using a polarization beam displacer and an iris. A beam sampling wedge (BSW) is used to create a sample of the incident power (I_s) of the interferometer chain. The measured incident beam sample is recorded during the experiment and used during post processing to both determine the actual time varying power at the input of the IFM chain and verify the variation is around ±10%. Additionally, the incident beam power was used to compensate for any fluctuations in the detector power caused by power fluctuations of the light source. The fluctuations in the light source can be caused by power supply variations, or by hopping between the different longitudinal laser modes. Next, the polarization is controlled with a quarter wave-plate (QWP) and half wave-plate. The QWP is used to remove the slight elliptical polarization caused by passing through BSW and reflecting off of M2.

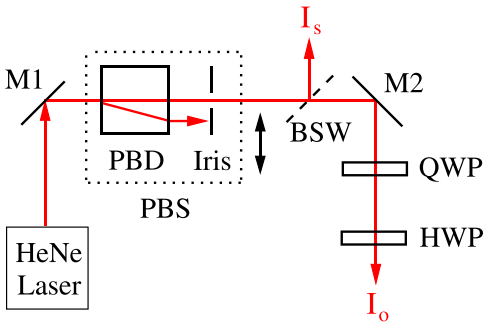

Figure 1. The polarization controlled light source used to supply light to the IFM experiments.

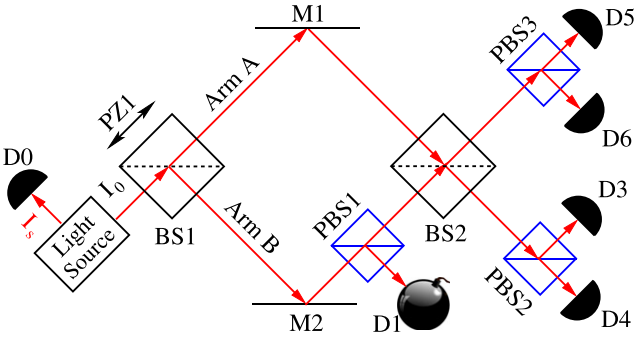

Figure 2. The setup for the single interferometer interaction free polarization measurement using vertically and horizontally polarized photons and polarization beam splitters to place the object in and out of the interferometer.

The single interferometer experimental setup for the simultaneous IFM consists of two non-polarizing beam splitters of approximately 20% reflectivity is shown in figure 2.

The first component in the interferometer is the non-polarizing beam splitter BS1. The measured reflection and transmission coefficients for the different polarizations and beam splitters BS1 and BS2 are given in table 1. The light in arm B reflects off of mirror M2 and goes through the polarization beam splitter PBS1. The vertically polarized light entering PBS1 is reflected into the photodiode 'bomb' D1 which effectively inserts the object into arm B. For horizontally polarized light PBS1 passes the light through it which

Table 1. Measured reflection and transmission coefficients of the three 30:70 beam splitters used in the experiment as measured with horizontally polarized laser at 632.8 nm.

Object	Reflection	Transmission	Loss	Polarization
BS1	18.4%	74.3%	7.3%	Horizontal
BS2	19.1%	73.9%	7.0%	Horizontal
BS3	21.8%	69.6%	8.6%	Horizontal
BS1	23.7%	67.1%	9.2%	Vertical
BS2	22.0%	71.9%	6.2%	Vertical
BS3	20.3%	69.5%	10.3%	Vertical
PBS1	0.0%	87.8%	12.2%	Horizontal
PBS1	86.4%	0.0%	13.6%	Vertical
PBS2	0.0%	85.8%	14.2%	Horizontal
PBS2	88.0%	0.0%	12.0%	Vertical

effectively removes the photodiode 'bomb' D1 from arm B. The power of the horizontal and vertical polarizations in both outputs of BS2 are measured using the polarization beam splitters PBS2, PBS3 and photodiodes D3–D6.

The horizontal light from arms A and B are combined at BS2. The observed interference at detectors D5 and D4 allows adjusting the interferometer phase to direct all the horizontally polarized light away from detector D5 and toward D4. The polarization beam splitter PBS1 inserts the 'bomb' D1 into arm B for vertically polarized photons. Therefore, the vertically polarized light in arm A has nothing to interfere with from arm B, so it splits at the beam splitter BS2 and propagates to both detectors D3 and D6. Since the interferometer is tuned to force all the light toward PBS2 when there is no 'bomb', a detection at D6 indicates the 'bomb' is in the interferometer. For diagonally polarized light (±45°), which contains both vertically and horizontally polarized photons, the 'bomb' will be measured to be both in and out of the interferometer depending on the photon polarization state measured at PBS1, PBS2 or PBS3.

3. Single interferometer experimental results

The following section presents the experimental results of the IFM chain experiment using a chain length of one.

The light incident on the system shown in figure 2 is linearly polarized at 45°. The relative phase difference between the two arms is varied using the piezo actuator PZ1. The measured power of the photodetectors versus the relative phase are displayed in figure 3. The interferometer relative path difference is zeroed when the light detected at D5 goes to zero.

For vertically polarized light the object D1 is present and absorbs 100% of the light incident upon it. This results in the quasi-dc signals for the vertically polarized light as measured by detector D3, object detector D1, and D6. The vertically polarized light detected at D3 represents light that yields no information about whether the object is in or out of the interferometer, since light always propagates toward PBS2 whether the object is present or not.

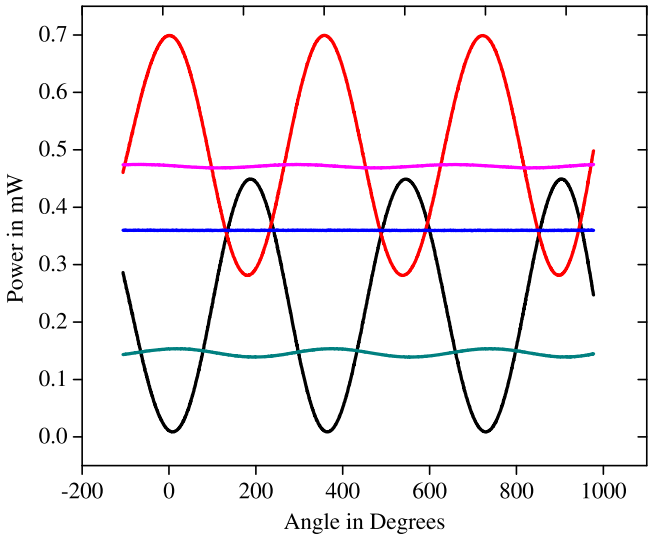

Figure 3. The measured power in milliwatts at the output of the single IFM chain for light linearly polarized at 45° as the relative path length between arms A and B are varied. The two sinusoidal waveforms from top to bottom are the horizontally polarized light detected by D4 and D5 respectively. The nearly flat lines from top to bottom, represent the vertically polarized light detected at D3, D1 and D6 respectively.

The light detected at D6 is an IFM $P_{\text{det}} = P_{D6}$, because it indicates the presence of the object without being absorbed by the object. The light detected in the object detector D1 represents the power absorbed by the object and is denoted by $P_{\text{abs}} = P_{D1}$. Since the power of the detected light is equivalent to the probability of detection of a single photon, the measure of the IFM efficiency [4] of the system can be found using equation (1)

$$\eta = \frac{P(\text{det})}{P(\text{det}) + P(\text{abs})}. \tag{1}$$

The experimental light measurements for 45° linearly polarized light are displayed in figure 3. The results for vertically polarized light show an IFM detection power (P_{det}) of 0.15 mW and the power absorbed by the object P_{abs} of 0.37 mW. Using equation (1), the IFM efficiency η is 28.8%. In an ideal lossless system, the ~20% reflective beam splitters would yield an IFM efficiency of $\eta = 44.4\%$.

The experimental results for the horizontally polarized component of the incident light (D4 and D5) are shown in figure 3. These results indicate there is no object in the system since the dark port D5 shows interference with visibility greater than 95% as the relative arm lengths are moved. This allows simultaneously measuring the IFM efficiency of the system as well as verifying that the relative interferometer arm lengths are correctly set if there were no object in the system. This avoids the need for an additional guide beam to simultaneously verify the relative phases of the interferometers when an object is present.

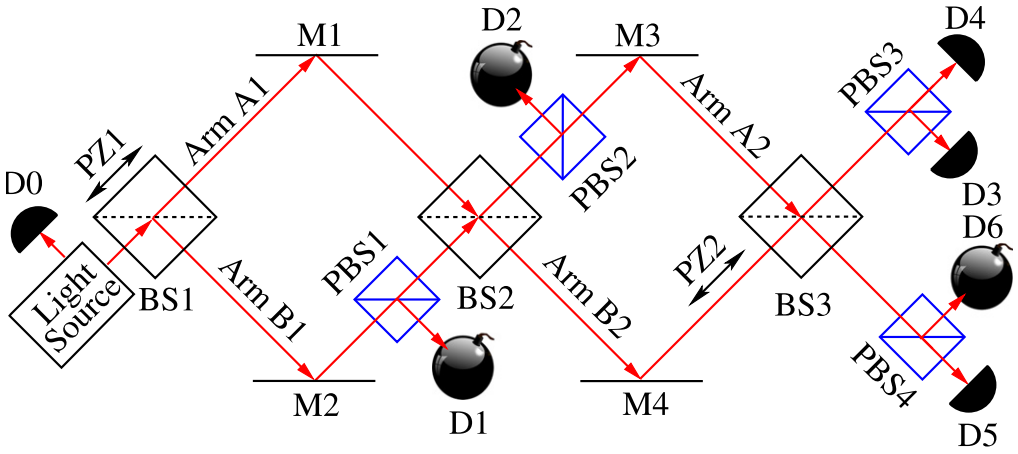

Figure 4. The experimental setup of the Mach–Zehnder interferometer IFM chain length of two using $N = 3$ beam splitters BS1, BS2, BS3. The PZ1 and PZ2 elements in the figure represent the piezoelectric actuators that are used to control the position of the beam splitters BS1 and BS3.

4. The two interferometer chain setup

The experimental setup for the interferometric chain of length two consists of the single interferometer chain with the addition of a polarization beam splitter PBS2, a non-polarizing beam splitter BS3 and two mirrors M3 and M4. The setup for the interferometer chain of length two is shown in figure 4. The number of beam splitters in the setup is represented by *N*. The object for IFM is located in arm A2 in the second interferometer instead of arm B2 as it would be for an interferometer chain with a greater than 50% beam splitter reflectivity. By locating the object in arm A2, the object will be exposed to the minimum amount of light since the reflected light is less than the transmitted light when the object D1 is in arm A1.

The second interferometer relative phase is adjusted by moving BS3 with a ceramic capacitor based nanomover PZ2 [11]. The two piezoelectric actuators allow independent control of the relative phase difference in both interferometers to allow all combinations of relative phase differences in the interferometer arms to be investigated. This allows investigating the phase combination of 90°, 180°, or 270° in the first interferometer. For this paper the phase of 180° in the first interferometer is chosen to investigate in detail. The ceramic capacitor based nanomover exhibits a nonlinear displacement versus applied voltage for applied voltages near zero volts, and near the maximum voltage. The data in the linear region will be what is used to compare the experimental results with the numerical simulation model of the system.

For horizontally polarized light, the object photodiodes D1, D2 and D6 are absent from the interferometer, which allows PZ1 and PZ2 to tune the relative phase in both interferometers to direct all the light to detector D5. For vertically polarized light, the object photodiodes D1, D2 and D5 are present in the interferometer and the light is directed to the photodetector D3.

5. Dual interferometer results

The following section presents the experimental results of the IFM chain experiment using a chain length of two. The IFM efficiency is compared between the single and double interferometer and also with the model. The photodetector measurements of detector D5 and the recursive phase model are compared.

Figure 5 displays the measured horizontally polarized light at the 'light port' detector D4 (top) and the 'dark port' detector D5 (bottom) as the relative path difference in the first and second interferometers are varied independently. The relative phase difference in the first interferometer is stepped from –32° to 379° in increments of 4.5°. The relative phase difference in the second interferometer is adjusted from 0° to 1440° then back to 0°. The second interferometer phase change results in the vertical lines at each phase of the first interferometer. This vertical nature is due to holding the phase of the first interferometer constant while the second interferometer phase is varied. The large phase change in the second interferometer allows capturing a region of nearly linear displacement versus PZ2 voltage which simplifies reconstructing the phase of the second interferometer from the measured detector power.

In figure 5, the maximum power in D5 occurs approximately when the first interferometer relative phase difference is 180° which is the optimum phase for IFM. There is a phase offset from the ideal 180° of approximately 8° caused by the lossy hybrid beam splitter coatings of BS1 and BS2. The phase offset from the first interferometer also causes the asymmetric (humps) in the horizontally polarized light measured by detector D4. The ability of the interferometer chain to detect the absence of an object depends upon adjusting the relative phases in the interferometers such that no light exits the system from D4. If the non-polarizing beam splitters have the same reflectivity for the horizontal and vertical polarizations, the horizontal polarization can be used to verify the interferometer chain phases are

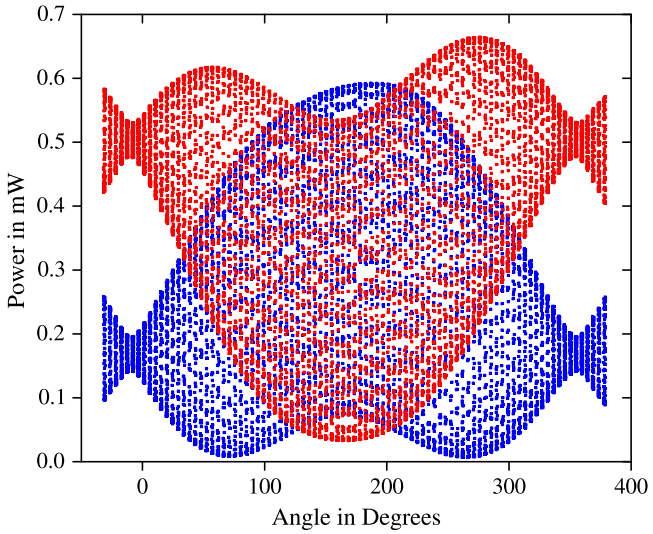

Figure 5. Plot of the power output of the chain length two IFM system in mW versus relative angular difference in the first interferometer. The detected horizontal power in detector D4 has two peaks and detector D5 has two minimums.

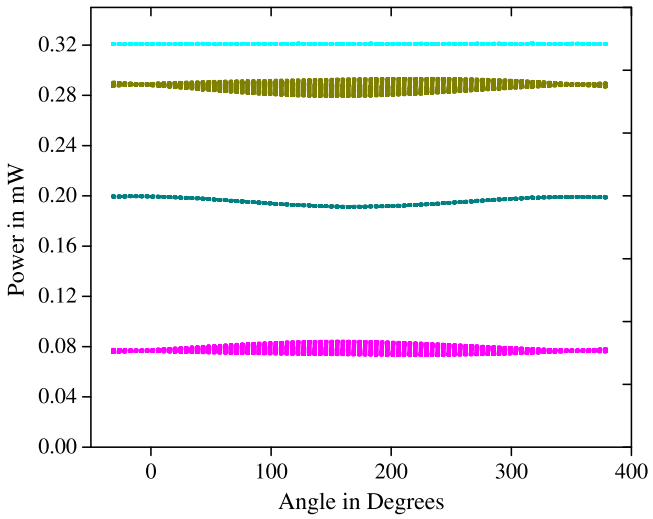

Figure 6. Plot of the vertical polarization output power in mW of the chain length two IFM system versus relative phase difference in the first interferometer. The detected power from the interferometer from top to bottom consists of the light absorbed by the object (D1), the light port (D3), the second object (D2) and the object in the dark port (D6). The photodetector D3 represents an interaction free measurement.

tuned to force all the light away from detector D4 to detector D5. The experimental setup is able to use interference to route all but 5% of the horizontally polarized light away from detector D4 into detector D5.

Vertically polarized light does not undergo interference since the arms of the interferometers with detectors D1 and D2 are opaque. Since interference forbids the light to go to PBS3 if the object is absent. An IFM P_{det} occurs when vertically polarized light is detected at D3 (P_{D3}). A detection at D3 indicates the presence of the object (D1, D2, and D6) without being absorbed by the object. The vertically polarized light measured by detectors D1, D3, D2, and D6 are plotted

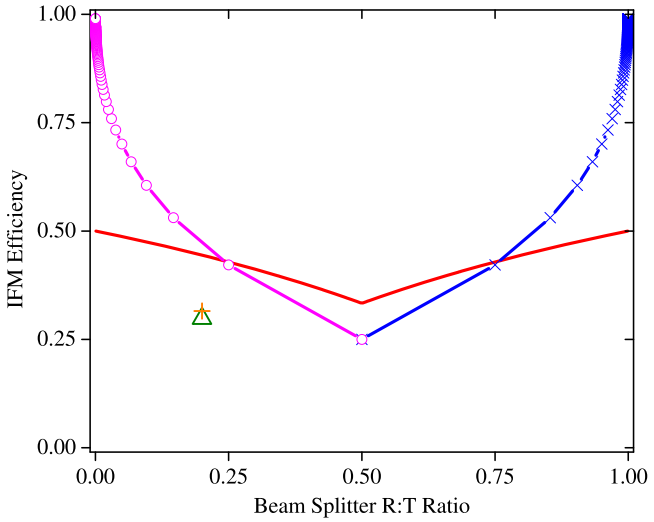

Figure 7. Comparison of the IFM efficiency measures for multiple interferometers as a function of beam splitter reflectivities. The IFM efficiency η for the EV interferometer is plotted as a solid line. The multiple interferometer chain IFM efficiency is plotted for reflectivities greater than 50% as a solid line with $\times$'s and a solid line with circles for reflectivities less than 50%. The 'o' in the middle represents a system with two beam splitters, the first 'o' ($\times$) to the left (right) represents three beam splitters ($N = 3$), etc. The experimental efficiency of the double (top) and single (below) interferometer IFM experiments are plotted as an '+' and an '$\triangle$' respectively.

in figure 6. The light detected in the object detectors D1, D2 and D5 are summed and represent the power absorbed by the object and are denoted as $P_{\text{abs}} = P_{D1} + P_{D2} + P_{D5} =$ .32 mW + .20 mW + .08 mW. Using equation (1) the IFM efficiency of the two interferometer system is $\eta_{N=3} = 31.8\%$.

The measurements shown in figures 5 and 6 were taken with incident light polarized at a 45° angle. If light polarized at 45° is incident on the interferometer chain, the interferometer arm lengths can be tuned to forbid horizontally polarized light to exit BS3 toward PBS3 while simultaneously the vertically polarized light is blocked by detectors D1 and D2 and allowed to pass through BS3 to PBS3. The slight variations in the power of the vertical light detectors in figure 6 are from the partial conversion of the horizontally polarized light subject to interference into vertically polarized light. The birefringence of the mirrors and beam splitters are responsible for this effect.

In order to model the experimental power at each photodetector and predict the IFM efficiency, all the optical components in the system are measured. The measured reflectivity, transmissivity and loss of the polarization dependent and independent beam splitters used in the experiment are listed in table 1.

6. IFM efficiency

The relationship between the ideal beam splitter reflectivity, the number beam splitters in the IFM chain N, and the IFM efficiency η is illustrated in figure 7 using equations (1), (3) and (4) as a function of beam splitter reflectivity. One point of

interest in comparing the IFM efficiencies of the single, and double interferometer setups is when the beam splitter reflectivity is 25%. The IFM efficiency of both lossless systems are approximately equal as measured with equation (1).

The IFM efficiency calculation predicts that an ideal lossless multiple interferometer system is more efficient in using photons than for a single interferometer when the number of beam splitters N is greater than three as plotted in figure 7. In addition to the theoretical IFM efficiency of a lossless system, figure 7 plots the two experimental data points for the double and single IFM chain experiments. The experimental efficiency is less due to losses in the mirrors M1–M4, beam splitters BS1–BS3, and the polarization beam splitters PBS1 and PBS2 [12]. A recursive phase model that can be used to predict the IFM chain experimental results with nonideal optics will now be discussed in detail.

6.1. Optimal reflectivity given N stages

The experimental IFM efficiency has been found for fixed beam splitter reflectivities for chain lengths of one and two. In order to predict the IFM efficiency for arbitrary reflectivities and any integer N beam splitters, a model of the interferometer chain is now presented. The model is compared with both the experimental efficiencies, and verifies the beam splitter transmissivity as a function of the IFM chain length equation (3) and its complement [4] yield the optimal reflectivity. The recursive model can find the probability of detecting photons in all the detectors given the optical system component properties. The IFM efficiency for arbitrary IFM chain lengths can be predicted using the recursive model.

The model is a recurrence relationship where the results of the current interferometer stage are dependent on the stage before it. This relationship is based on complex phasor arithmetic [13] describing the interference of two plane waves.

$$
\begin{aligned}
a_A(0) &= 0,\\
a_B(0) &= \sqrt{P_0},\\
a_A(N) &= t'_A(N)\{a_A(N-1)\exp\\
&\quad \times [\mathrm{i}\theta(N)]r_A(N) + a_B(N-1)t(N)\},\\
a_B(N) &= t'_B(N)\{a_A(N-1)\\
&\quad \times \exp[\mathrm{i}\theta(N)]t(N) + a_B(N-1)r_B(N)\},\\
P_A(N) &= a_A(N)a_A^*(N),\\
P_B(N) &= a_B(N)a_B^*(N),\\
t(N) &= \sqrt{T(N)},\\
r_A(N) &= \sqrt{R(N)}\exp[\mathrm{i}(\pi+\phi)],\\
r_B(N) &= \sqrt{R(N)},\\
T'_A(N) &= 100\%,\ 85\%,...,\\
T'_B(N) &= 85\%,\ 100\%,...,\\
t'_A(N) &= \sqrt{T'_A(N)},\\
t'_B(N) &= \sqrt{T'_B(N)}.
\end{aligned}
\tag{2}
$$

The recursive formula in equation (2) describes the interference that occurs at a beam splitter N in the interferometer chain. The amplitude of the light output from the Nth beam splitter in the A arm and the B arm is denoted by $a_A(N)$ and $a_B(N)$ respectively. The light power in the upper and lower arms of the interferometer after the Nth beam splitter is defined as $P_A(N)$ and $P_B(N)$ respectively. The variables $R(N)$ and $T(N)$ are the reflectivity and transmissivity of the Nth beam splitter with respect to power. The reflectivity in terms of amplitude for the A and B arms is given by $r_A(N)$ and $r_B(N)$ respectively. The π phase shift in the $r_A(N)$ term represents the phase shift due to light in the 'A' arm reflecting from the Nth beam splitter. The reflection term $r_B(N)$ represents the reflection from the beam splitter incident from the bottom and without a phase shift. The variable $t(N)$ indicates the transmissivity of each beam splitter as measured in amplitude. The angle $\theta(N)$ represents the relative phase difference between the two arms of the interferometer. The phase between the reflected and transmitted light ϕ is to account for the phase difference caused by the loss in each beam splitter BS(N). The transmission coefficients of the object polarization beam splitters PBS(N) in the arms of each interferometer stage are $T'_A(N)$ and $T'_B(N)$.

The optimal reflectivity to perform the IFM experiment given an arbitrary number N of beam splitters can be found with the model using three constraints. The first constraint is that when no object is in the system it must be possible to output all of the light in the dark port. The second constraint is that the reflectivity is near zero in the case of reflectivity less than 50% and near one in the case it is above 50%. The third constraint is that the relative phase differences in each of the interferometers must be optimized to transfer the light from the light to the dark port. A plot of the probability of light exiting the dark port for a two interferometer system ($N = 3$) beam splitters as the beam splitter reflectivity is varied is shown in figure 8. From this graph the optimal reflectivities occur at 25% and 75% which confirms the prediction of equation (3). The dark port is arm B for the 25% reflectivity and switches to arm A for the 75% reflectivity. The swapping of exit arms versus reflectivity occurs when N is an odd number greater than one. For an even number of beam splitters N greater than two, the dark port is always arm A for any reflectivity. For a more complicated IFM system, the number of beam splitters N is set to 20. A plot of the probability of light going into the dark port versus beam splitter reflectivity is given in figure 9. The optimal reflectivity near zero is 0.615%. The optimal reflectivity near one is 99.385%. In this plot, there are multiple reflectivities where all the light can be directed to the dark port (arm A).

The reflectivities that direct all the light to the dark port are the same as the optimal reflectivities predicted by equations (3) and (4) for $1 < N <= 20$ and N is even. This is due to the light completely interfering into arm B one or more times as it traverses the interferometer system. For example the optimal reflectivity for $N = 4$ will cause the light to completely interfere into arm B five times as it traverses the 20 beam splitters. For the optimal IFM reflectivity, the light

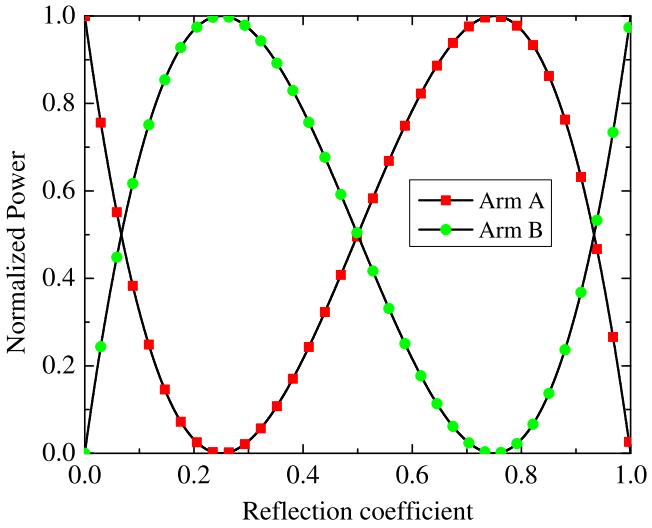

Figure 8. Three beam splitter Mach–Zehnder IFM interferometer chain (two interferometers) theoretical intensity versus beam splitter reflection coefficient. The dark port is arm B if the reflectivity is less than 50%, and is arm A for reflectivity greater than 50%. The normalized power is plotted against the beam splitter reflectivity. The only reflectivities that can be used to perform IFM are where arm A can be tuned to unity or zero. The reflectivities of 0 and 1 are not valid for IFM measurements since it is not possible to have interference for these reflectivities.

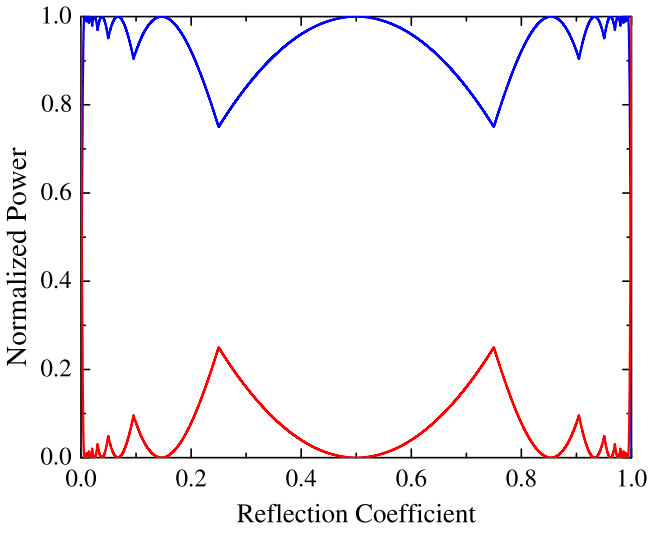

Figure 9. The model predicted dark (top) and light (bottom) port power versus beam splitter reflection coefficient for a twenty beam splitter Mach–Zehnder IFM interferometer chain. All twenty of interferometers in the chain have a relative phase difference of 180°. An interferometer chain with 20 beam splitters gives a theoretical IFM efficiency of 88% that matches the efficiency obtained by Namekata [14] using a Fabry Pérot etalon.

transfers completely to the dark port only at the last beam splitter in the chain.

For a transmissive IFM chain with beam splitter reflectivity of less than 50%, equation (3) can be used to find the best beam splitter transmission coefficient given N beam splitters in the IFM system. The optimal reflectivity found with the model for $N = 3$ for the transmissive and reflective IFM chains are 75%, and 25% respectively. The optimal transmissivities and reflectivities agree with both equations (3) and (4). These equations are the complement of those given by Kwiat *et al* [4] since their theoretical experimental model used beam splitter reflectivities with greater than 50% reflectivity

$$T(N) = \cos^2\left(\frac{\pi}{2N}\right), \tag{3}$$

$$R(N) = \sin^2\left(\frac{\pi}{2N}\right). \tag{4}$$

The optimal reflectivity is found using the recursive model to plot the probability of light exiting the light and dark ports as the reflectivity of the beam splitters is varied. If the reflectivity is decreased beyond the optimal value for N, the adjustment of the relative phase difference between the two interferometer stages does not allow all the light to exit the dark port. If the reflectivity is increased beyond the optimal amount, the relative phase difference between the arms can be adjusted to send all the light to the dark port of the output of the interferometer chain. The IFM efficiency increases as the reflection coefficient decreases in the case of a transmissive type multistage IFM setup. For some applications such as imaging where a small percent of false detection is allowed, the overall IFM efficiency can be increased. If the reflectivity of the mirrors is reduced from the optimal value some of the light will exit the light port falsely indicating the presence of an object. However, for an IFM chain with $N = 3$, and a 1% false object detection rate the reflectivity of the mirrors can be reduced by 11.3% from the optimal 25% to a reflection coefficient of 22.2% in a lossless system. By decreasing the reflectivity, the IFM efficiency will increase from 42% to 47% since the probability of light hitting the object is reduced.

6.2. Comparison between experiment and model

The recursive model of the interferometer chain uses experimentally determined phases, reflectivity and transmissivity for modeling the optical components in the system as shown in table 1. The results of plotting the recursive model for the dark port (D5) with horizontally polarized light is shown in figure 10. The recursive model prediction agrees well the actual photodiode power measurement. The horizontal axis indicates the phase difference between the arms of the first interferometer is varied from –20° to 380°. While the phase in the first interferometer is held constant, the phase of the second interferometer is varied from 0° to 1440° and back to 0°. The reason for varying the phase of the second interferometer by multiple wavelengths is to allow capturing a single wavelength of linear displacement versus voltage region of the piezoactuator PZ2 [11, 15]. The linear displacement allows low order polynomial curve fitting of the phase of both interferometers from the experimental photodiode power measurements using a genetic algorithm [16]. A genetic algorithm was chosen since it is robust against signal noise and works well with finding the polynomial coefficients.

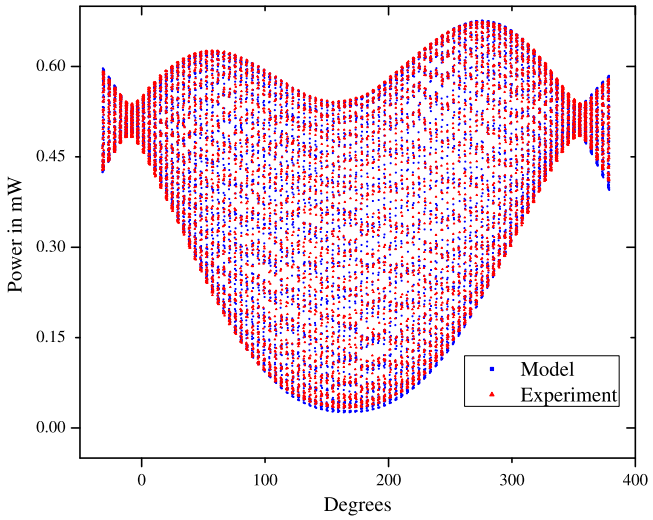

Figure 10. Plot of the recursive model and experimental results of a two interferometer IFM chain of the the horizontal photodiode power in the 'light port' D4. The vertical axis is the photodiode power in mW, and the horizontal axis is the relative phase difference between the arms of the first interferometer. The vertical lines of dots represent the possible light power levels due to the combination of interference in the first and second interferometers. The theory and model agree well enough to be not discernable in the plot.

7. Discussion and conclusion

The chain of interferometers as discussed in this paper uses beam splitters with less than 50% reflectivity. This choice of reflectivity forces the object location to alternate between the upper and lower arms of the interferometer chain. For the highest efficiency IFM the beam splitter reflectivities need to be near zero. The choice of lower than 50% reflectivity has the advantage of allowing the beam splitter ratios to be arbitrarily close to zero by adjusting the incident angle to make use of Brewster's angle. This allows changing the length N of the IFM chain for horizontally polarized incident light more feasible than having the beam splitters manufactured with a fixed ratio in advance for each chain length.

Another potential use of the interferometer chain is to investigate the effect caused by combinations of objects present or absent in the dark port of any interferometer in the chain. For an IFM chain of length N it may be possible to encode a binary number of N bits by either having an object or not in any combination of interferometer arms This could be used to implement an optical key lock where the individual mechanical tumblers are replaced with interferometer arms and the key would block the correct combination of arms to get the output light amplitude and phase to unlock. For an optical key lock it would be interesting to use an object capable of electromagnetically induced transparency [17] to input a key pattern without requiring a physical object to be moved. The IFM chain also has potential use in counterfactual computation such as Grover's algorithm [18] or quantum logic gates [19].

In conclusion this paper has investigated an IFM chain of interferometers method using beam splitter reflectivities less than 50%, and an object that exists or not depending on the incident light polarization. The ability to move the object in and out of a chain of interferometers without physical motion makes IFM chains more feasible to implement. For diagonally polarized light the object can be measured to be in the measurement arms while simultaneously allowing diagnosis of the IFM chain phases without the object. The proposed recursive model agrees well with the measured experimental data and can be used to model arbitrary chain length IFM systems to improve efficiency.

Acknowledgments

The authors acknowledge discussions with Donald Bord and financial support from the University of Michigan Office of the Vice President Research.

References

[1] Renninger M 1960 *Z. Phys.* **158** 417–21
[2] Dicke R H 1981 *Am. J. Phys.* **49** 925–30
[3] Elitzur A and Vaidman L 1993 *Found. Phys.* **23** 987–97
[4] Kwiat P, Weinfurter H, Herzog T, Zeilinger A and Kasevich M A 1995 *Phys. Rev. Lett.* **74** 4763–6
[5] Conkey D B, Brown A N, Caravaca-Aguirre A M and Piestun R 2012 *Opt. Express* **20** 4840–9
[6] Ma X s, Guo X, Schuck C, Fong K Y, Jiang L and Tang H X 2014 *Phys. Rev.* A **90** 042109
[7] Chirolli L, Strambini E, Giovannetti V, Taddei F, Piazza V, Fazio R, Beltram F and Burkard G 2010 *Phys. Rev.* B **82** 045403
[8] Wolfgramm F, de Icaza Astiz Y A, Beduini F A, Cerè A and Mitchell M W 2011 *Phys. Rev. Lett.* **106** 053602
[9] Bonadeo N H, Erland J, Gammon D, Park D, Katzer D S and Steel D G 1998 *Science* **282** 1473–6
[10] Matres J, Ballesteros G, Mas S, Brimont A, Sanchis P, Marti J and Oton C 2014 *IEEE J. Sel. Top. Quantum Electron.* **20** 417–21
[11] Wang J, Elghoul G and Peters S 2013 *IEEE Trans. Ultrason. Ferroelectr. Freq. Control* **60** 256–60
[12] Kwiat P G, White A G, Mitchell J R, Nairz O, Weihs G, Weinfurter H and Zeilinger A 1999 *Phys. Rev. Lett.* **83** 4725–8
[13] Hecht E 2001 *Optics* 4th ed (Reading, MA: Addison-Wesley)
[14] Namekata N and Inoue S 2006 *J. Phys. B: At. Mol. Opt. Phys.* **39** 3177
[15] Hall D A 2001 *J. Mat. Sci.* **36** 19
[16] Goldberg D E 1989 *Genetic Algorithms in Search, Optimization and Machine Learning* 1st edn (Boston, MA: Addison-Wesley)
[17] Wang J 2010 *Phys. Rev.* A **81** 033841
[18] Hosten O, Rakher M T, Barreiro J T, Peters N A and Kwiat P G 2006 *Nature* **439** 949–52
[19] Huang Y P and Moore M G 2008 *Phys. Rev.* A **77** 062332